



# Self-Discharge Induced Stress and Associated Mechanical Damage in Na-Ion Battery Electrodes

A. Alfadhli<sup>1</sup> · A. S. Pakhare<sup>1</sup> · V. A. Sethuraman<sup>2</sup> · S. P. V. Nadimpalli<sup>1</sup>

Received: 24 December 2025 / Accepted: 4 March 2026  
© The Author(s) 2026

## Abstract

**Background** Self-discharge is known to cause chemical degradation in batteries; however mechanical behavior of electrode materials during self-discharge process has not been explored.

**Objective** This study aims to investigate potential evolution and stress development in electrodes due to self-discharge process, and to assess the effect of self-discharge induced stresses on the electrode performance.

**Methods** Germanium thin film electrodes were cycled against Na under galvanostatic and self-discharge conditions. A multibeam optical sensor (MOS) integrated with a custom electrochemical cell was used to carry out operando stress measurements during galvanostatic and self-discharge processes; a subsequent SEM analysis of the samples was carried out to assess the influence of stresses on mechanical integrity.

**Results** During ~ 165 h of self-discharge, the potential evolved continuously from a fully sodiated state of 5 mV to 1.2 V vs. Na/Na<sup>+</sup>, indicating continuous loss of stored sodium-ions from Ge. As a result, electrode stresses evolved continuously throughout the OCP, changing from a compressive value of -0.5 GPa at the start of OCP to a tensile stress value of 0.71 GPa, i.e., a total stress change of 1.2 GPa without any external agency applying forces on the electrode. A prolonged (i.e., more than ~ 100 h) exposure to high tensile stress causes electrode fracture (mechanical damage).

**Conclusions** Self-discharge not only causes irreversible electrochemical parasitic losses but also promotes mechanical damage in high volume expansion electrodes if not addressed properly. Hence, to develop high performance electrodes for rechargeable batteries, electrochemical measurements should be coupled with mechanical characterization.

**Keywords** Self-discharge · Electrode stress · Mechanical degradation · *In-situ* measurement · Sodium-ion batteries

## Introduction

Self-discharge is a process in which a fully charged battery, when stored, i.e., not connected to any load or device, slowly loses its charge over time. All primary and secondary batteries undergo self-discharge to some extent (i.e., they lose stored energy when not in use) and at different rates. For instance, lithium-ion batteries typically experience a self-discharge of about 2% of their charge capacity per month [1]. Nickel-metal hydride (Ni-MH) batteries exhibit a higher self-discharge rate, typically about 20–25%

per month [2]. On the other hand, lead-acid batteries display a wider range, with rates varying from 2–5% and 15–25% per month, depending on the age of the battery [3]. One of the main mechanisms responsible for self-discharge is the parasitic reactions between electrode and electrolyte [4–6], especially the passivation layer (or Solid Electrolyte Interface, SEI) formation.

An ideal SEI film on the surface of the electrodes should be stable, thin, electronically insulating, and ionically conductive [7–9]. This layer, when reaches a sufficient thickness, adds kinetic stability and prevents further decomposition of the electrolyte [10]. However, SEI layers on many electrodes may not be continuous and could be unstable due to different electrolyte characteristics [9, 11–13], which leads to continuous parasitic reactions causing self-discharge (i.e., consumption of the stored ions). For example, sodium (Na) salt was found to form unstable SEI compared to those

✉ S. P. V. Nadimpalli  
sivan@msu.edu

<sup>1</sup> Mechanical Engineering, Michigan State University, East Lansing, MI 48824, USA

<sup>2</sup> Department of Chemical Engineering, University of South Carolina, Columbia, SC 29208, USA

formed in the presence of lithium (Li) and potassium (K) salts [14].

There has been a lot of focus on the self-discharge mechanisms and optimization of the electrolyte/electrode combinations of various battery chemistries. However, all the reports in the existing literature have focused mainly on the electrochemical aspects of the self-discharge problem. These studies have contributed towards understanding the chemical degradation such as loss of lithium inventory via SEI formation/dissolution/reformation. However, they did not consider implications of self-discharge process on the mechanical behavior of electrodes. For example, as the self-discharge process leads to concentration changes within an active material, it could lead to electrode stresses.

Previous reports demonstrated experimentally that the concentration changes in electrodes lead to volume expansion-induced stresses. For example, Ge electrodes can expand up to 239% when fully sodiated [15] and 260% when fully lithiated [16], and Si expands up to 400% upon lithiation [17]. This level of volume expansion can induce a significant amount of stress in the battery electrodes. Sethuraman et al., [18] Bucci et al., [19] Al-Obedi et al., [20] Nadimpalli et al., [21] Rakshit et al., [22] Pharr et al., [23] and Soni et al., [24] have measured electrode stresses experimentally and reported that the stresses could reach as high as 1.5 GPa. Stress is the driving force for mechanical degradation, such as fracture of electrodes which contributes to capacity fade [25–28]. In addition, stresses also affect the equilibrium potential [18], reaction kinetics [29, 30], and transport processes [31]. Hence, it is imperative to understand if stresses develop in electrodes during self-discharge, and to ascertain if the self-discharge induced stresses lead to mechanical damage. Despite the importance of electrode stresses and their influence on electrochemical and mechanical processes in electrodes, no study exists on the mechanical behavior of electrodes during self-discharge phenomenon. Understanding this is especially crucial for the large volume change (next generation high energy density) electrodes.

Therefore, the objective here was to carry out real-time stress measurements during self-discharge process of large volume change (high energy density) electrodes and to ascertain if these stresses cause any mechanical damage. To this end, Na-based electrode and electrolyte system was chosen as a model system to study this phenomenon. Specifically, Ge thin film was chosen as the working electrode, 1 M of NaClO<sub>4</sub> in propylene carbonate (PC) with 5% fluoroethylene carbonate (FEC) additive as the electrolyte, and Na foil as the counter/reference electrode. An optical-based experimental apparatus integrated with an electrochemical cell was used to perform in-operando stress measurements during self-discharge and regular electrochemical cycling. It should be noted that the Ge electrode used in this study is a

nonporous and binder-less electrode without any conductive additives, i.e., a solid thin film electrode, and it eliminates all the geometric and structural complexities of a composite electrode and leads to tractable stress and electrochemical measurements. Note that the focus here is to investigate the relation between self-discharge process and the electrode stress development and to understand if these stresses cause any associated mechanical damage of electrode. The framework proposed here is more general and applicable to any electrode/electrolyte system.

## Experimental Method

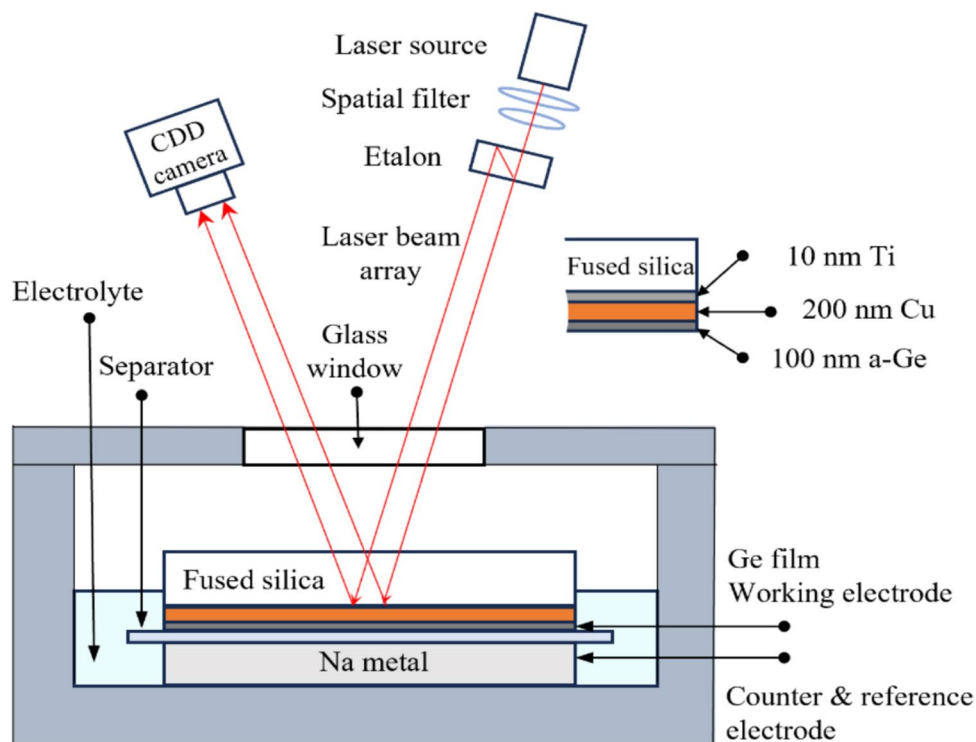
### Ge Thin Film Electrode and Electrochemical Cell Preparation

Germanium films of ~100 nm thickness were sputter deposited on a double-side polished fused silica (SiO<sub>2</sub>) substrates (thickness ~500 μm, diameter ~5.08 cm) that have been coated with ~5 nm of Ti (for better adhesion) and ~200 nm of Cu (as a current collector). In addition, the Ge film was also deposited on a thin Cu sheet (thickness ~150 μm) to use in coin cells. The thickness of the deposited films was measured with a stylus profilometer. The Ge film was deposited using (Kurt J Lesker Axis system) DC sputtering technique with 65 W power over 2 in diameter target at 3mTorr of Ar gas, resulting in a deposition rate of ~1 Å/s. The Ge films deposited under these conditions are known to be amorphous [32]. The Raman spectra obtained on these sputter-deposited Ge thin films (Fig. S1) show a broad peak, indicating the amorphous nature of the sputter-deposited Ge films.

Figure 1 shows the schematic of the electrochemical cell made of a Teflon beaker. The amorphous germanium (a-Ge) film was used as the working electrode, while a 2 mm thick sodium foil (that was prepared from Na cubes 99% trace metals basis from Sigma Aldrich) was used as the counter/reference electrode. The electrolyte consists of 1 M sodium perchlorate (NaClO<sub>4</sub>, >98% pure, Sigma Aldrich) in propylene carbonate (PC, 99.7% anhydrous, Sigma Aldrich) with a 5 wt.% fluoroethylene carbonate (FEC, Sigma Aldrich) as an additive [33]. A glass microfiber sheet (Grade GF/C, pore size ~1.2 μm, Sigma Aldrich) was used as the separator to prevent physical contact between the electrodes. Coin cells (i.e., CR2032) were also prepared with the same electrode/electrolyte combination. Since no curvature measurements are performed in a coin cell, the a-Ge film deposited on a Cu foil was used as working electrode here. All the cells, i.e., both beaker and coin cells, were assembled inside a glovebox (MBraun Inc.) filled with Argon and maintained at <0.1 ppm of O<sub>2</sub> and <0.1 ppm of H<sub>2</sub>O.

The beaker cell shown in Fig. 1 was subjected to electrochemical cycling using a Solartron 1470E potentiostat.

**Fig. 1** The schematic of the electrochemical cell and the multibeam optical sensor (MOS) setup. The inset shows the details of electrode sample



The Ge electrodes were cycled under three different electrochemical conditions: (i) galvanostatic (i.e., at a constant current density of  $i = 6 \mu\text{A cm}^{-2}$  corresponding to  $\sim C/3.25$ ) sodiation/desodiation cycling between 2 V and 0.005 V vs.  $\text{Na}/\text{Na}^+$ , (ii) a single galvanostatic sodiation/desodiation cycle followed by a galvanostatic sodiation until the potential reaches 0.005 V vs.  $\text{Na}/\text{Na}^+$  and then allowing self-discharge to occur under an open circuit potential (OCP) condition for prolonged period (i.e., typically for more than 150 h) until potential reached 1.2 V vs.  $\text{Na}/\text{Na}^+$ , and (iii) a single galvanostatic sodiation to a potential of 0.005 V vs.  $\text{Na}/\text{Na}^+$  followed by a self-discharge (or an open circuit) condition just like (ii). The first experiment enables measurement of baseline electrode behavior during regular cycling while the second and third experiments are self-discharge experiments. All these beaker cell experiments were conducted inside the glove box; the current, potential, and stresses response of the electrode were measured continuously throughout these experiments.

In addition to the beaker cell, some coin cell experiments were carried out under the same protocols mentioned above (i.e., (i), (ii), and (iii) conditions discussed above) primarily to characterize the electrochemical behavior of Ge electrodes in a more standard coin cell configuration and to compare that with the results from the beaker cell experiments mentioned above. The coin cells are also subjected to extensive cycling; for example, galvanostatic cycling with  $i = 6 \mu\text{A cm}^{-2}$  for forty-seven cycles between 2 V and 0.005 V vs.  $\text{Na}/\text{Na}^+$ . Further, the a-Ge film electrodes in coin cell, after

undergoing self-discharge, were galvanostatically desodiated to 2 V vs.  $\text{Na}/\text{Na}^+$  to estimate/quantify the capacity loss due to self-discharge. Besides these galvanostatic cycling and self-discharge experiments, the coin cells were also subjected to (a) cyclic voltammetry (CV) experiments at a scan rate of  $0.1 \text{ mV s}^{-1}$  between 2 V and 5 mV vs.  $\text{Na}/\text{Na}^+$  and (b) the galvanostatic intermittent titration technique (GITT) to estimate the equilibrium potential of the a-Ge electrode as a function of Na concentration. The experimental protocol (with GITT step at various capacities) is shown in Fig. S2.

### SEM Analysis

Scanning electron microscopy (SEM) analysis was performed on the as-deposited and self-discharged a-Ge film electrodes to understand the effect of self-discharge process on the mechanical integrity of the electrode films. The beaker cells were disassembled inside the glove box and samples were rinsed with propylene carbonate (PC) and immediately placed in a sealed container filled with argon gas before moving them out of the glove box. This was done to minimize the exposure to oxygen during transportation, and the samples were quickly transferred into the SEM chamber.

### Stress Measurements using the Multibeam Optical Sensor (MOS)

The schematic in Fig. 1 illustrates the multi-beam optical sensor (MOS) setup that was used to monitor changes in the

curvature of a fused silica substrate during electrochemical cycling and self-discharge process of the a-Ge film. The MOS setup includes a laser source with a central wavelength of 660 nm, a single collimated beam, and two etalons. This arrangement was used to produce a  $2 \times 2$  array of laser beams, which were directed toward the sample, as shown in Fig. 1. A CCD camera captured the reflected laser beams from the sample, and the resulting image appears as a  $2 \times 2$  array of circular dots on a computer monitor. The sample curvature,  $\kappa$ , change is determined by measuring the change in spacing between the laser beams (or circular dots). Note from Fig. 1, that the Na foil, glass fiber separator, and a-Ge films remained submerged in the electrolyte throughout the experiment, while the surface of the substrate was not submerged. This avoids laser passes through the electrolyte.

The stress in the a-Ge film can be determined by

$$\sigma = \sigma_r + \frac{E_s t_s^2 k}{6 t_f (1 - \nu_s)} \quad (1)$$

(Stoney's equation) [34–36], which relates substrate curvature,  $\kappa$ , to film stress,  $\sigma$ . Here  $E_s$ ,  $t_s$ , and  $\nu_s$  are Young's modulus, thickness, and Poisson's ratio of the fused silica ( $\text{SiO}_2$ ) substrate, respectively, while  $t_f$  represent the a-Ge film thickness. The parameter  $\sigma_r$  is the residual stress of the as-prepared a-Ge film that is caused by the mismatch in thermal expansion between the a-Ge film and the fused silica substrate during the deposition process. It should be noted that the stress values reported here are based on the original thickness  $t_f$  of the a-Ge film and is the nominal stress in the film (i.e.,  $t_f$  is constant).

## Results and Discussion

### Electrochemical and Stress Response of a-Ge Film during Regular Cycling

Figure 2 shows the cyclic voltammogram (CV) of the a-Ge thin-film electrode cycled against a sodium reference electrode for the first five cycles (from the coin cell experiments). A slight increase in the current at  $\sim 0.8$  V vs.  $\text{Na}/\text{Na}^+$  during the first cathodic sweep (i.e., sodiation of the pristine a-Ge film) which was absent in all the subsequent cycles can be attributed to the formation of the solid electrolyte interphase layer. The sharp increase in current at  $\sim 85$  mV vs.  $\text{Na}/\text{Na}^+$  during the first cathodic sweep is attributed to the sodium alloying reaction with germanium. Note that the potential associate with this sharp increase shifted to the right during subsequent cathodic sweeps, and the peak current value also increased with cycling (i.e., the number of electrons involved in the reaction increases [37]), suggesting improved reaction kinetics. The anodic sweep has a single peak corresponds to

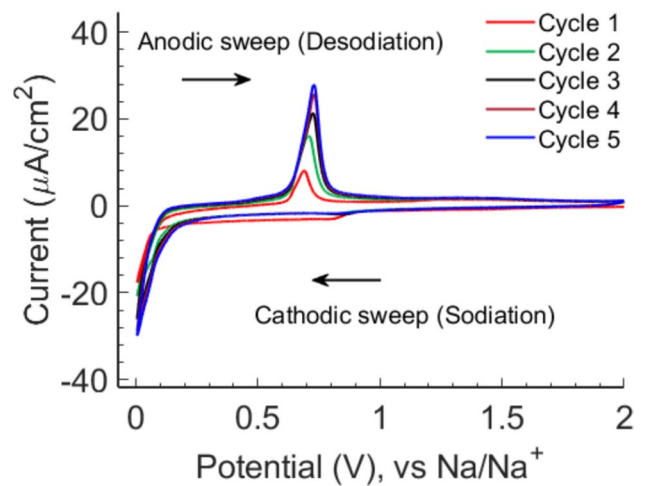
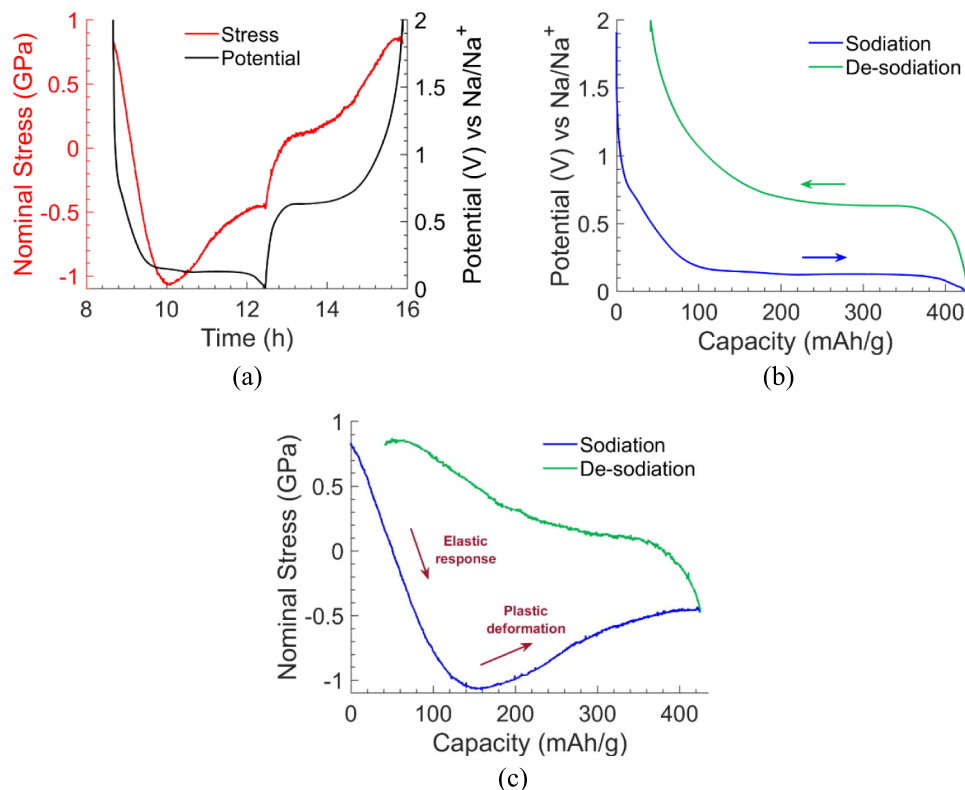


**Fig. 2** Cyclic voltammogram (CV) of a-Ge film cycled against Na foil with a sweeping rate of 1 mV/s showing the characteristic sodiation/desodiation peaks

the desodiation of the a-Ge film. The peak associated with this reaction is centered at  $\sim 0.68$  V vs.  $\text{Na}/\text{Na}^+$  for the first cycle but shifted to right reaching  $\sim 0.73$  V vs.  $\text{Na}/\text{Na}^+$  for the fifth cycle, while the peak values increased with each cycle, suggesting improved electrochemical kinetics. These observations are in agreement with the previous reports on a-Ge films cycled against Na [15].

Figure 3a shows the potential and stress response of the a-Ge film during a typical galvanostatic (i.e., a constant current density of  $6 \mu\text{A cm}^{-2}$  corresponding to  $\sim C/3.25$  rate) sodiation/desodiation cycle with respect to time (data from second cycle). The same data, i.e., potential and stress, is presented in Fig. 3b and c, respectively, as a function of capacity. Note from Fig. 3a and b, that upon sodiation (i.e., when sodium reacts with Ge) the potential decreases sharply from 2 to approximately 0.8 V vs.  $\text{Na}/\text{Na}^+$ , but decreases gradually afterwards to 0.1 V vs.  $\text{Na}/\text{Na}^+$  (owing to SEI formation which is more predominant below 0.8 V vs.  $\text{Na}/\text{Na}^+$ ). The potential then remains almost constant at 0.1 V vs.  $\text{Na}/\text{Na}^+$  with time (and capacity) until the end of sodiation. The long plateau near 0.1 V vs.  $\text{Na}/\text{Na}^+$ , corresponds to Na alloying with the a-Ge film. At the end of the sodiation process, the potential drops rapidly to the cutoff voltage of 5 mV vs.  $\text{Na}/\text{Na}^+$  at  $425 \text{ mAh g}^{-1}$ . Upon desodiation, the potential rises sharply to  $\sim 0.6$  V vs.  $\text{Na}/\text{Na}^+$  and remains constant until a capacity of  $200 \text{ mAh g}^{-1}$  and increasing rapidly thereafter as desodiation continues to  $41 \text{ mAh g}^{-1}$ . Note that the plateau around 0.6 V vs.  $\text{Na}/\text{Na}^+$  aligns with the Na extraction peak shown in Fig. 2. The capacity loss during the cycle is primarily attributed to side reactions (e.g., SEI layer formation), and a majority of the SEI film forms during the first cycle [38–40]. The Ge electrodes were also cycled under the same galvanostatic conditions in a standard coin

**Fig. 3** (a) Shows the stress and potential response of a-Ge thin film electrode as a function of time; (b) and (c) show the potential and stress response, respectively, as a function of specific capacity during galvanostatic sodiation/desodiation cycling



cell configuration; the electrochemical data and observations from both coin cell (see Fig. S3) and beaker cell experiments agree well with the reported data by Zhang et al. [41], Baggetto et al. [42], and Rakshit et al. [15].

Figures 3a and c show the nominal stress response of the a-Ge electrode as a function of time and capacity, respectively, during regular galvanostatic sodiation/desodiation cycling ( $C/3.25$  rate). Upon sodiation, i.e., when sodium is inserted into a-Ge matrix, the stress which is  $\sim 0.8$  GPa at the start of the cycle changes linearly with capacity and becomes compressive. Note that the compressive stress is indicated as negative stress and tensile stress is indicated as positive stress. The sodium insertion into Ge matrix leads to expansion, but the elastic substrate constrains the expansion inducing compressive stress. As the sodiation continues, the stress increases linearly with capacity toward compressive, attaining a peak value of  $-1.07$  GPa at a capacity of  $158 \text{ mAh g}^{-1}$ , decreases with capacity there after reaching a value of  $-0.47$  GPa at the end of sodiation ( $425 \text{ mAh g}^{-1}$ ). The linear stress variation with capacity at the beginning of sodiation is due to elastic response and the subsequent non-linear response is due to irreversible plastic deformation. As soon as the desodiation process begins, i.e., when sodium is removed from Ge matrix, the stress becomes tensile and increases linearly at the beginning followed by nonlinear response, mirroring the behavior observed during sodiation process. The stress returns to the original tensile value at

the end of desodiation process. This behavior is consistent with the previous report by Rakshit et al. [15]. The results presented in Fig. 3 establish a quantitative baseline for the coupled electrochemical and mechanical behavior of a-Ge during a regular galvanostatic sodiation/desodiation cycling.

### Electrochemical and Mechanical Response of Ge Electrode during Self-Discharge and the Associated Damage

Figure 4a shows the stress and potential response of a-Ge film during a full galvanostatic cycle followed by a second sodiation step, an open-circuit potential (OCP) period where self-discharge was allowed to proceed, and a third sodiation step. The data corresponding to the self-discharge (or OCP) step is shown in Fig. 4b separately for clarity. Note that the data during regular galvanostatic steps in Fig. 4a matches with the data presented in Fig. 3, i.e., standard galvanostatic cycling. During the OCP, i.e., when the electrodes are disconnected, the potential is expected to relax to a steady state value (not far from  $\sim 5$  mV in the present case). However, it can be noted from Fig. 4b, that the electrode potential has evolved continuously throughout the approximately 165 h of OCP (or self-discharge). At the start of OCP (i.e., immediately after the second sodiation) when the a-Ge electrode is almost saturated with Na, the potential has increased relatively quickly to  $\sim 0.6$  V vs.  $\text{Na/Na}^+$  within the first few

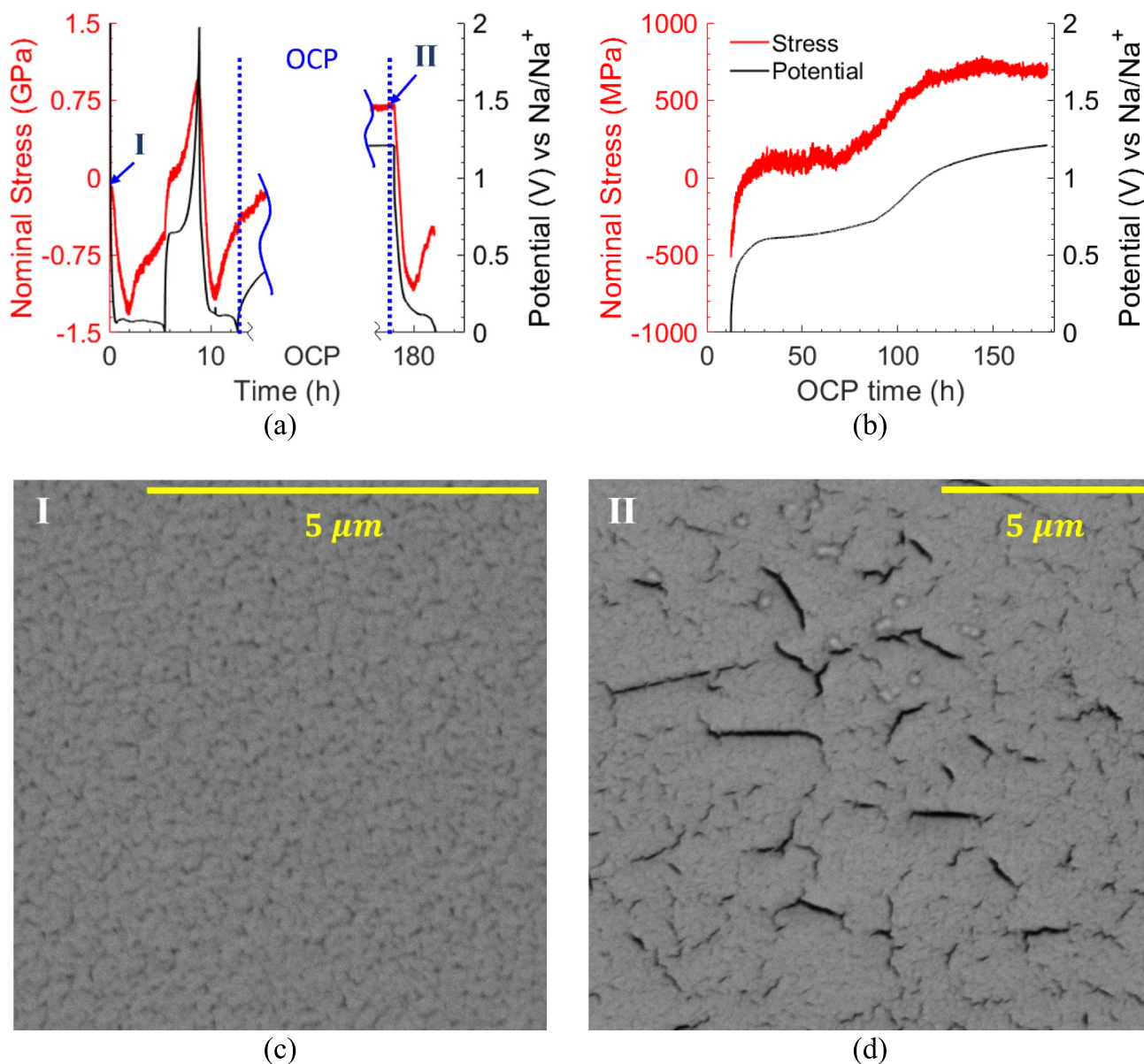


**Fig. 4** (a) Shows the potential and stress response during a regular galvanostatic cycle, second galvanostatic sodiation, and the final sodiation process; the data between the two dashed lines is plotted in (b) which corresponds to the sample response during OCP (or Self-discharge process). (c) and (d) show the SEM images of Ge thin film electrode before electrochemical cycling and after the self-discharge process, respectively (i.e., at I and II indicated in “a”). The interesting point to note here is that the electrode which was under OCP (i.e., disconnected and not in use) from 11 h developed cracks due to self-discharge induced stresses

hours. The potential then remained almost constant for the next 75 h; note that the rate of increase of potential during this stage is very small but not zero. After about 100 h the potential again starts to increase gradually with time and reaches another plateau potential around 1.2 V vs. Na/Na<sup>+</sup>. This behavior was consistent among four samples tested in beaker cell configuration and four samples tested in coin cell configuration. The continuous change in potential is a clear indication that the sodium is leaving germanium due to

self-discharge process, and the fact that the electrode spent a significant amount of time (i.e., more than 80 h) at the ~0.65 V vs. Na/Na<sup>+</sup> which according to the CV data from Fig. 2 is close to the potential corresponding to desodiation process supports this hypothesis.

A more interesting and surprising data is the electrode stress presented in Fig. 4b. As mentioned earlier, the stress response of electrodes during self-discharge process was not studied before, and Fig. 4b shows, for the first time, how

electrode stresses evolve during a self-discharge process. Note from the figure that the stress in NaGe electrode at the beginning of the self-discharge (or OCP) process was 500 MPa of compression. Since the electrodes are disconnected during an OCP and are assumed to be under equilibrium conditions, it is expected that the stress remains constant. However, it is interesting to see (from Fig. 4b) that the electrode stress changed continuously throughout the OCP step. This can be attributed to the fact that the self-discharge reaction drives concentration changes in the electrode, which induces stress change. Note that as soon as the electrode is subjected to OCP, stress started relaxing, i.e., stress changes rapidly with time from a compressive stress of 500 MPa in the beginning to a tensile stress value of  $\sim 100$  MPa within the first 17 h of OCP step. The electrode stress then remains almost constant at this level for the next 60 h, and then increased with time with further OCP reaching a tensile value of 0.71 GPa. The electrode stress remains constant at this high tensile value of 0.71 GPa until about 165 h. The surprising fact here is that all this stress change, i.e., from a compressive value of  $-0.5$  GPa at the start of OCP to a tensile stress value of 0.71 GPa, occurred without any external agency applying forces on the electrode.

The stress relaxation phenomenon (i.e., stress changes with time without the influence of any external agency) is quite common in materials [43–45] (metals, polymers, ceramics, amorphous materials, and composites); for example, when a polymeric material is subjected to a constant strain and left alone (such as the Ge electrode which is sodiated completely and left alone, i.e., OCP), stress relaxes to a constant steady state value (usually close towards zero stress). However, what is interesting to see in Fig. 4b is that when the electrode is left alone, i.e., under OCP, the stress did not relax to a steady state value, but it increased with time and became tensile without the help of any external agency applying forces on the electrode. What this means is that when a fully charged cell is (unused) sitting on a shelf, the (negative) electrodes will develop tensile stresses due to self-discharge process. Although no external forces are acting on the electrode, the thermodynamic driving force for self-discharge reaction in Na-Ge (to cause concentration changes in the electrode) is strong enough to induces tensile stresses in the electrode (self-discharge chemistry and mechanical coupling). In fact, the driving force is strong enough to produce a tensile stress as high as 0.71 GPa after about 165 h of OCP when the electrode potential reaches almost 1.2 V vs. Na/Na<sup>+</sup>. This is a significant observation, because what this experiment has demonstrated is that during self-discharge, the electrode stresses could reach tensile stresses of the order of a GPa. Such level of large tensile stresses lead to fracture and mechanical damage.

To understand if the self-discharge induced stresses caused any mechanical damage, SEM analysis was

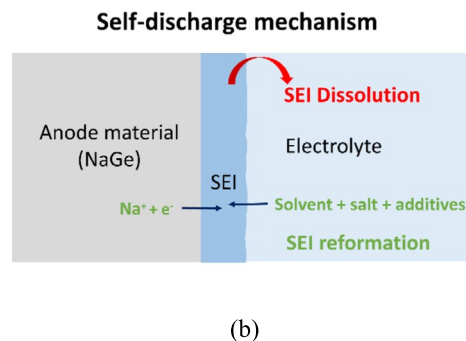
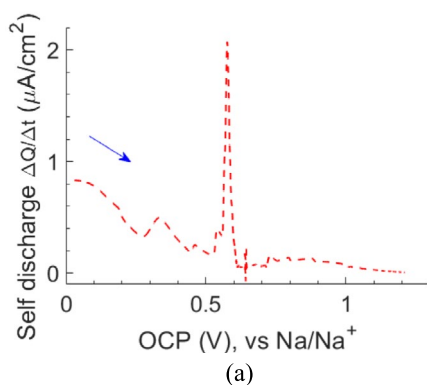
conducted on the electrodes at different stages of cycling and are presented in Figs. 4c and d. Note that the pristine a-Ge electrode shown in Fig. 4c has no visible cracks, but the SEM image of the sample after self-discharge process in Fig. 4d (and Fig. S4) shows numerous cracks confirming our hypothesis that self-discharge induced tensile stresses caused mechanical damage. It should be noted that Rakshit et al. [15] demonstrated experimentally that during a regular galvanostatic cycling when the peak tensile stress was close to 1 GPa, no cracking was observed in the first few cycles. However, a slightly lower stress of 0.71 GPa during a single self-discharge process led to fracture of Na-Ge electrode. This can be attributed to the time dependent deformation mechanism such as creep. Since the sodiated Ge is an amorphous material, creep deformation mechanisms are important [43–45], i.e., besides the high tensile stress magnitude, the amount of time the electrode is exposed to these high stress levels is also very important. For example, during a regular galvanostatic cycle (i.e., in Rakshit et al. [15] and in Fig. 3) although the electrode experienced  $\sim 1$  GPa of stress without experiencing cracks because it was only for few minutes; however, during the self-discharge the electrode is subjected to tensile stress of 0.71 GPa for several hours (i.e., close to 100 h). The materials which are susceptible to creep tend to relax moderately high tensile stresses by developing cracks as shown in Fig. 4d [46, 47]. Hence, time-dependent deformation mechanisms such as creep makes the self-discharge induced tensile stresses more detrimental than the peak tensile stresses induced during regular galvanostatic cycling.

### Self-discharge Mechanisms and Reactions Rates

Although the primary focus of this work is to understand the effect of self-discharge process on the mechanical behavior of electrodes, it is useful to see how the self-discharge rate evolves with potential. The capacity (or charge) loss information is required to estimate reaction rates and is typically determined either by running a charge or a discharge process after the OCP step [5, 6, 48–51]. However, a relation between potential and the content (or amount) of sodium in the electrode, along with the data from Fig. 4b, can also provide both the charge loss and the rate at which capacity is lost. Fig. S2 describes the details of this method.

Figure 5a depicts how the self-discharge rate (i.e., kinetics) and potential (thermodynamics) are related. Note that the self-discharge (or charge loss) rate is  $0.9 \mu\text{A}/\text{cm}^2$  at the beginning and decreases with potential throughout the OCP except at 0.6 V vs. Na/Na<sup>+</sup>, where it attains a peak value of more than  $2 \mu\text{A}/\text{cm}^2$ . This peak self-discharge rate correlates with the desodiation reaction peak of the Na-Ge system shown in the CV plot in Fig. 2. Data obtained from a coin cell experiment (presented in Fig. S5) also agrees very well

**Fig. 5** (a) The self-discharge rate as a function of OCP. (b) A schematic showing the self-discharge mechanism, where an unstable SEI forms on the electrode during cycling and undergoes concurrent dissolution and reformation at the expense of the stored charge during OCP



with this data. The primary factor contributing to self-discharge is the instability of the passivation (SEI) layer, leading to its dissolution and reformation, which results in the continuous reduction of electrolyte solvents at the expense of stored charge [5, 6, 52–54]. The schematic in Fig. 5b illustrates the process of SEI layer dissolution and reformation, driving self-discharge. As the existing SEI layer dissolves, the system favors the formation of a new SEI at the electrode–electrolyte interface [55]. Hence, the self-discharge rate is affected by (i) the dissolution rate of passivation layer, (ii) the kinetics of SEI reformation, and (iii) the potential of the electrode (or Na content within the electrode).

Since the dissolution rate of the SEI compounds may be independent of the electrode potential or the Na content in the electrode, the self-discharge rate may be primarily governed by the electrode potential (or Na content) and the SEI reformation kinetics. The relatively higher self-discharge rate observed at the beginning of the OCP step can be attributed to the fact that the Na content in the electrode is at the highest and the voltage of the electrode is favorable for SEI formation. Note that the equilibrium potential for SEI formation is 0.9 V vs. Na/Na<sup>+</sup> [56], and the driving force for SEI formation increases as the potential goes below this value. Also, the stable compound between Na and Ge is NaGe [57, 58], i.e.,  $x = 1$  in Na<sub>x</sub>Ge; however, consistent with the reports from literature, metastable compounds with  $x > 1$  are formed at the higher Na concentrations. Hence, a combination of the strong driving force for SEI formation and to form a stable NaGe compound, can be attributed to the high self-discharge rate at the beginning. The driving force for SEI formation decreases as the potential increases, which is consistent with the data in Fig. 5a. Further, it is clear from the CV curve shown in Fig. 2 that desodiation is thermodynamically favored at 0.6 V vs Na/Na<sup>+</sup>, and at this potential SEI formation is still favorable; hence, a combination of these two conditions resulted in the peak self-discharge rate at this potential. A comparison of potential as a function of sodium content, during a regular galvanostatic desodiation process and a self-discharge (or OCP) process is

presented in Fig. S6a, and it shows that the overall potential trend is similar in both cases, with slightly lower potential values during self-discharge conditions due to the absence of overpotential. The close similarity of data between self-discharge and galvanostatic desodiation conditions indicates that self-discharge follows the same thermodynamic pathways as desodiation, but the rate of reaction is different. As shown in Fig. 5a, the rate of charge leaving the electrode (or self-discharge rate) varies throughout the self-discharge step as opposed to a constant rate (or current prescribed) during galvanostatic desodiation. The same analyses conducted in a coin cell configuration (Fig. S5) is consistent with this data.

## Conclusions

Mechanical behavior of a large volume expansion sodium-ion battery anode material was investigated during a self-discharge process (i.e., the process in which the stored energy is lost over time when batteries are left alone and unused). The a-Ge was used as a model electrode for the study. Operando measurement of electrode potential and stresses were carried out during regular and self-discharge processes. The stress and potential response of the Ge electrode during regular galvanostatic cycling agreed well with the observations and data from the earlier reports. During self-discharge (or OCP), the potential evolved continuously from a fully sodiated state of 5 mV vs. Na/Na<sup>+</sup> to 1.2 V vs. Na/Na<sup>+</sup>, indicating continuous loss of stored sodium-ions from germanium. It was observed that the self-discharge rate was relatively higher at the beginning of the OCP and decreased continuously throughout the OCP process except at 0.6 V vs. Na/Na<sup>+</sup> where self-discharge rate was the highest. Since the desodiation is thermodynamically favored at 0.6 V vs Na/Na<sup>+</sup> and SEI formation is still favorable at this potential, a combination of these two conditions is attributed to the peak self-discharge rate at this potential.

The more interesting result is the electrode stress evolution during self-discharge. When the fully sodiated

germanium at  $-0.5$  GPa of compressive stress was subjected to OCP, stress started relaxing immediately, i.e., stress changed rapidly with time initially to reach tensile stress value of  $\sim 100$  MPa within the first 17 h of OCP step and remained almost constant at this level for the next 60 h, and thereafter it increased with time reaching a tensile value of 0.71 GPa. The electrode stress remains constant at this high tensile value of 0.71 GPa until about 165 h of OCP. The surprising fact here is that all this stress change of more than 1.2 GPa, i.e., from a compressive value of  $-0.5$  GPa at the start of OCP to a tensile stress value of 0.71 GPa, occurred without any external agency applying forces on the electrode. Further, a tensile stress of 0.71 GPa during self-discharge, which is slightly lower than the peak tensile stress that occurs in regular galvanostatic cycle, caused fracture and mechanical damage.

In summary, this study shows that the self-discharge process not only leads to loss of sodium inventory towards irreversible SEI reactions but also leads to significant tensile stresses in the electrodes that cause fracture. The concentration changes that occur due to self-discharge process led to continuous evolution of stresses in the electrode reaching tensile levels on the order of GPa. Besides the high magnitude, the amount of time the electrode is subjected to these high tensile stresses makes the self-discharge induced stresses more detrimental than those induced during regular galvanostatic cycling. These moderately high tensile stresses during self-discharge nucleate and propagate cracks, i.e., mechanically degrading the electrode material, even when it is not actively cycled electrochemically. The amorphous materials such as NaGe are prone to creep deformation mechanisms, and a prolonged exposure to a moderate level of tensile stress could lead to cracking. Hence, if self-discharge-mechanical coupling is not properly addressed, especially in the large volume change materials, electrodes will be damaged without even cycling. Hence, to be able to develop next generation high performance electrodes for rechargeable batteries or to develop optimized electrolyte chemistry, stress analysis should be coupled with electrochemical measurements.

**Supplementary Information** The online version contains supplementary material available at <https://doi.org/10.1007/s11340-026-01289-z>.

**Acknowledgements** Authors would like to acknowledge partial funding from the National Science Foundation through grant# CMMI-2026717. SN would like to acknowledge partial support from G. Glenn and Marlene D. Gardner Endowed Faculty Scholarship from Michigan State University. Authors thank Dr. Subhjit Rakshit for initial help with this project.

**Author Contributions** Abdulrahman Alfidhli: Methodology, Validation, Formal analysis, Investigation, Visualization, Writing-original draft;

Akshay S Pakhare: Investigation;

Vijay A Sethuraman: Methodology, Supervision; and

Siva P V Nadimpalli: Conceptualization, Methodology, Resources, Writing-review and editing, Supervision, Project administration, and Funding acquisition.

**Funding** National Science Foundation grant# CMMI-2026717 and G. Glenn and Marlene D. Gardner Endowed Faculty Scholarship from Michigan State University.

**Data Availability** Data will be available upon request.

## Declarations

**Ethical Approval** Not applicable.

**Consent to Participate and Consent to Publish** Not applicable.

**Competing interests** Not applicable.

**Open Access** This article is licensed under a Creative Commons Attribution 4.0 International License, which permits use, sharing, adaptation, distribution and reproduction in any medium or format, as long as you give appropriate credit to the original author(s) and the source, provide a link to the Creative Commons licence, and indicate if changes were made. The images or other third party material in this article are included in the article's Creative Commons licence, unless indicated otherwise in a credit line to the material. If material is not included in the article's Creative Commons licence and your intended use is not permitted by statutory regulation or exceeds the permitted use, you will need to obtain permission directly from the copyright holder. To view a copy of this licence, visit <http://creativecommons.org/licenses/by/4.0/>.

## References

- Nagasubramanian G, Doughty D (2001) Improving the interfacial resistance in lithium cells with additives. *J Power Sources* 96:29–32. [https://doi.org/10.1016/S0378-7753\(01\)00498-0](https://doi.org/10.1016/S0378-7753(01)00498-0)
- Kularatna N (2011) Rechargeable batteries and their management. *IEEE Instrum Meas Mag* 14:20–33. <https://doi.org/10.1109/MIM.2011.5735252>
- Garche J (2009) Encyclopedia of electrochemical power sources. Elsevier, Acad. Press, Amsterdam
- Yazami R, Reynier Y (2002) Mechanism of self-discharge in graphite–lithium anode. *Electrochim Acta* 47:1217–1223. [https://doi.org/10.1016/S0013-4686\(01\)00827-1](https://doi.org/10.1016/S0013-4686(01)00827-1)
- Sinha NN, Smith AJ, Burns JC et al (2011) The use of elevated temperature storage experiments to learn about parasitic reactions in wound LiCoO<sub>2</sub>/Graphite cells. *J Electrochem Soc* 158:A1194. <https://doi.org/10.1149/2.007111jes>
- Buechele S, Logan E, Boulanger T et al (2023) Reversible self-discharge of LFP/Graphite and NMC811/Graphite cells originating from redox shuttle generation. *J Electrochem Soc* 170:010518. <https://doi.org/10.1149/1945-7111/acb10c>
- Muñoz-Márquez MÁ, Saurel D, Gómez-Cámer JL et al (2017) Na-ion batteries for large scale applications: a review on anode materials and solid electrolyte interphase formation. *Adv Energy Mater* 7:1700463. <https://doi.org/10.1002/aenm.201700463>
- Wu J, Ihsan-Ul-Haq M, Chen Y, Kim J-K (2021) Understanding solid electrolyte interphases: advanced characterization techniques and theoretical simulations. *Nano Energy* 89:106489. <https://doi.org/10.1016/j.nanoen.2021.106489>
- Li B, Chao Y, Li M et al (2023) A review of solid electrolyte interphase (SEI) and dendrite formation in lithium

- batteries. *Electrochem Energy Rev* 6:7. <https://doi.org/10.1007/s41918-022-00147-5>
10. Peled E (1979) The electrochemical behavior of alkali and alkaline earth metals in nonaqueous battery systems—the solid electrolyte interphase model. *J Electrochem Soc* 126:2047–2051. <https://doi.org/10.1149/1.2128859>
  11. Adenusi H, Chass GA, Passerini S et al (2023) Lithium batteries and the solid electrolyte interphase (SEI)—progress and outlook. *Adv Energy Mater* 13:2203307. <https://doi.org/10.1002/aenm.202203307>
  12. Yildirim H, Kinaci A, Chan MKY, Greeley JP (2015) First-principles analysis of defect thermodynamics and ion transport in inorganic SEI compounds: LiF and NaF. *ACS Appl Mater Interfaces* 7:18985–18996. <https://doi.org/10.1021/acsami.5b02904>
  13. Shen X, Zhang R, Chen X et al (2020) The failure of solid electrolyte interphase on Li metal anode: structural uniformity or mechanical strength? *Adv Energy Mater* 10:1903645. <https://doi.org/10.1002/aenm.201903645>
  14. Moshkovich M, Gofer Y, Aurbach D (2001) Investigation of the electrochemical windows of aprotic alkali metal (Li, Na, K) salt solutions. *J Electrochem Soc* 148:E155. <https://doi.org/10.1149/1.1357316>
  15. Rakshit S, Pakhare AS, Ruiz O et al (2021) Measurement of volume changes and associated stresses in Ge electrodes due to Na/Na<sup>+</sup> redox reactions. *J Electrochem Soc* 168:010504. <https://doi.org/10.1149/1945-7111/abd5fc>
  16. Liang W, Yang H, Fan F et al (2013) Tough germanium nanoparticles under electrochemical cycling. *ACS Nano* 7:3427–3433. <https://doi.org/10.1021/nn400330h>
  17. Jerliu B, Hüger E, Dörrer L et al (2014) Volume expansion during lithiation of amorphous silicon thin film electrodes studied by in-operando neutron reflectometry. *J Phys Chem C* 118:9395–9399. <https://doi.org/10.1021/jp502261t>
  18. Sethuraman VA, Srinivasan V, Bower AF, Guduru PR (2010) In situ measurements of stress-potential coupling in lithiated silicon. *J Electrochem Soc* 157:A1253. <https://doi.org/10.1149/1.3489378>
  19. Bucci G, Nadimpalli SPV, Sethuraman VA et al (2014) Measurement and modeling of the mechanical and electrochemical response of amorphous Si thin film electrodes during cyclic lithiation. *J Mech Phys Solids* 62:276–294. <https://doi.org/10.1016/j.jmps.2013.10.005>
  20. Al-Obeidi A, Kramer D, Thompson CV, Mönig R (2015) Mechanical stresses and morphology evolution in germanium thin film electrodes during lithiation and delithiation. *J Power Sources* 297:472–480. <https://doi.org/10.1016/j.jpowsour.2015.06.155>
  21. Nadimpalli SPV, Tripuraneni R, Sethuraman VA (2015) Real-time stress measurements in Germanium thin film electrodes during electrochemical lithiation/delithiation cycling. *J Electrochem Soc* 162:A2840–A2846. <https://doi.org/10.1149/2.0941514jes>
  22. Rakshit S, Tripuraneni R, Nadimpalli SPV (2018) Real-time stress measurement in SiO<sub>2</sub> thin films during electrochemical lithiation/delithiation cycling. *Exp Mech* 58:537–547. <https://doi.org/10.1007/s11340-017-0371-2>
  23. Pharr M, Choi YS, Lee D et al (2016) Measurements of stress and fracture in germanium electrodes of lithium-ion batteries during electrochemical lithiation and delithiation. *J Power Sources* 304:164–169. <https://doi.org/10.1016/j.jpowsour.2015.11.036>
  24. Soni SK, Sheldon BW, Xiao X, Tokranov A (2011) Thickness effects on the lithiation of amorphous silicon thin films. *Scr Mater* 64:307–310. <https://doi.org/10.1016/j.scriptamat.2010.10.003>
  25. Nadimpalli SPV, Sethuraman VA, Bucci G et al (2013) On plastic deformation and fracture in Si films during electrochemical lithiation/delithiation cycling. *J Electrochem Soc* 160:A1885–A1893. <https://doi.org/10.1149/2.098310jes>
  26. Szczech R, Jin J (2011) Nanostructured silicon for high capacity lithium battery anodes. *Energy Environ Sci* 4:56–72. <https://doi.org/10.1039/C0EE00281J>
  27. Besenhard JO, Yang J, Winter M (1997) Will advanced lithium-alloy anodes have a chance in lithium-ion batteries? *J Power Sources* 68:87–90. [https://doi.org/10.1016/S0378-7753\(96\)02547-5](https://doi.org/10.1016/S0378-7753(96)02547-5)
  28. Beaulieu LY, Eberman KW, Turner RL et al (2001) Colossal reversible volume changes in Lithium alloys. *Electrochem Solid-State Lett* 4:A137. <https://doi.org/10.1149/1.1388178>
  29. Bucci G, Chiang Y-M, Carter WC (2016) Formulation of the coupled electrochemical–mechanical boundary-value problem, with applications to transport of multiple charged species. *Acta Mater* 104:33–51. <https://doi.org/10.1016/j.actamat.2015.11.030>
  30. Yang H, Liang W, Guo X et al (2015) Strong kinetics-stress coupling in lithiation of Si and Ge anodes. *Extreme Mech Lett* 2:1–6. <https://doi.org/10.1016/j.eml.2014.11.008>
  31. Tripuraneni R, Rakshit S, Nadimpalli SPV (2018) In situ measurement of the effect of stress on the chemical diffusion coefficient of Li in high-energy-density electrodes. *J Electrochem Soc* 165:A2194. <https://doi.org/10.1149/2.0641810jes>
  32. Laforge B, Levan-Jodin L, Salot R, Billard A (2007) Study of germanium as electrode in thin-film battery. *J Electrochem Soc* 155:A181. <https://doi.org/10.1149/1.2820666>
  33. Purushotham U, Takenaka N, Nagaoka M (2016) Additive effect of fluoroethylene and difluoroethylene carbonates for the solid electrolyte interphase film formation in sodium-ion batteries: a quantum chemical study. *RSC Adv* 6:65232–65242. <https://doi.org/10.1039/C6RA09560G>
  34. (1909) The tension of metallic films deposited by electrolysis. *Proc R Soc Lond Ser Contain Pap Math Phys Character* 82:172–175. <https://doi.org/10.1098/rspa.1909.0021>
  35. Sethuraman VA, Chon MJ, Shimshak M et al (2010) In situ measurements of stress evolution in silicon thin films during electrochemical lithiation and delithiation. *J Power Sources* 195:5062–5066. <https://doi.org/10.1016/j.jpowsour.2010.02.013>
  36. Chen C-H, Chason E, Guduru PR (2017) Numerical solution of moving phase boundary and diffusion-induced stress of Sn anode in the lithium-ion battery. *J Electrochem Soc* 164:E3661. <https://doi.org/10.1149/2.0661711jes>
  37. Marken F, Neudeck A, Bond AM (2002) Cyclic Voltammetry. In: Scholz F (ed) *Electroanalytical methods: guide to experiments and applications*. Springer, Berlin, Heidelberg, pp 51–97
  38. Nadimpalli SPV, Sethuraman VA, Dalavi S et al (2012) Quantifying capacity loss due to solid-electrolyte-interphase layer formation on silicon negative electrodes in lithium-ion batteries. *J Power Sources* 215:145–151. <https://doi.org/10.1016/j.jpowsour.2012.05.004>
  39. Patil A, Patil V, Wook Shin D et al (2008) Issue and challenges facing rechargeable thin film lithium batteries. *Mater Res Bull* 43:1913–1942. <https://doi.org/10.1016/j.materresbull.2007.08.031>
  40. An SJ, Li J, Daniel C et al (2016) The state of understanding of the lithium-ion-battery graphite solid electrolyte interphase (SEI) and its relationship to formation cycling. *Carbon* 105:52–76. <https://doi.org/10.1016/j.carbon.2016.04.008>
  41. Zhang J, Zheng T, Cheng KE et al (2023) Insights into the sodiation kinetics of Si and Ge anodes for sodium-ion batteries. *J Electrochem Soc* 170:100518. <https://doi.org/10.1149/1945-7111/ad0075>
  42. Baggetto L, Keum JK, Browning JF, Veith GM (2013) Germanium as negative electrode material for sodium-ion batteries. *Electrochem Commun* 34:41–44. <https://doi.org/10.1016/j.elecom.2013.05.025>
  43. Meyers MA, Chawla KK (2008) *Mechanical behavior of materials*, 2. ed., 4. print. with corr. Cambridge University Press, Cambridge

44. Courtney TH (2005) Mechanical behavior of materials: Second edition. Waveland Press
45. Dieter GE (2000) Mechanical metallurgy, 3. ed., 14. [print.]. McGraw-Hill, Boston, Mass.
46. Kassner ME, Hayes TA (2003) Creep cavitation in metals. *Int J Plast* 19:1715–1748. [https://doi.org/10.1016/S0749-6419\(02\)00111-0](https://doi.org/10.1016/S0749-6419(02)00111-0)
47. Goods SH, Nix WD (1978) The kinetics of cavity growth and creep fracture in silver containing implanted grain boundary cavities. *Acta Metall* 26:739–752. [https://doi.org/10.1016/0001-6160\(78\)90024-X](https://doi.org/10.1016/0001-6160(78)90024-X)
48. Mogensen R, Brandell D, Younesi R (2016) Solubility of the solid electrolyte interphase (SEI) in sodium ion batteries. *ACS Energy Lett* 1:1173–1178. <https://doi.org/10.1021/acseenergylett.6b00491>
49. Broussely M, Herreyre S, Biensan P et al (2001) Aging mechanism in Li ion cells and calendar life predictions. *J Power Sources* 97:13–21. [https://doi.org/10.1016/S0378-7753\(01\)00722-4](https://doi.org/10.1016/S0378-7753(01)00722-4)
50. Ma LA, Buckel A, Hofmann A et al (2023) Fundamental understanding and quantification of capacity losses involving the negative electrode in sodium-ion batteries. *Adv Sci* 11:2306771. <https://doi.org/10.1002/advs.202306771>
51. Zhu WH, Zhu Y, Tatarchuk BJ (2014) Self-discharge characteristics and performance degradation of Ni-MH batteries for storage applications. *Int J Hydrog Energy* 39:19789–19798. <https://doi.org/10.1016/j.ijhydene.2014.09.113>
52. Madi Reddy SK, Shang W, White RE (2022) Mathematical model for SEI growth under open-circuit conditions. *J Electrochem Soc* 169:090505. <https://doi.org/10.1149/1945-7111/ac8ee5>
53. Wang C, Zhang X, Appleby AJ (2002) Self-discharge of secondary lithium-ion graphite anodes. *J Power Sources* 112:98–104. [https://doi.org/10.1016/S0378-7753\(02\)00359-2](https://doi.org/10.1016/S0378-7753(02)00359-2)
54. Ramasamy RP, Lee J-W, Popov BN (2007) Simulation of capacity loss in carbon electrode for lithium-ion cells during storage. *J Power Sources* 166:266–272. <https://doi.org/10.1016/j.jpowsour.2006.12.086>
55. Xu K (2014) Electrolytes and interphases in Li-ion batteries and beyond. *Chem Rev* 114:11503–11618. <https://doi.org/10.1021/cr500003w>
56. Ji Y, Qiu J, Zhao W et al (2023) In situ probing the origin of interfacial instability of Na metal anode. *Chem* 9:2943–2955. <https://doi.org/10.1016/j.chempr.2023.06.002>
57. Okamoto H (2014) Supplemental literature review of binary phase diagrams: Al-Br, B-Cd, Cd-Mg, Cd-Ti, Er-Fe, Fe-Nd, Ge-Na, Ge-Ni, Ge-Sc, Hf-W, Pb-Yb, and Re-Ti. *J Phase Equilib Diffus* 35:195–207. <https://doi.org/10.1007/s11669-013-0273-7>
58. Wang Y, Wang P, Zhao D et al (2012) Thermodynamic description of the Ge–Na and Ge–K systems using the CALPHAD approach supported by first-principles calculations. *Calphad* 37:72–76. <https://doi.org/10.1016/j.calphad.2012.01.004>

**Publisher's Note** Springer Nature remains neutral with regard to jurisdictional claims in published maps and institutional affiliations.